

Spider-Web-Inspired Stretchable Graphene Woven Fabric for Highly Sensitive, Transparent, Wearable Strain Sensors

Xu Liu,^{†,||} Dan Liu,^{†,||} Jeng-hun Lee,[†] Qingbin Zheng,^{*,†,‡} Xiaohan Du,[†] Xinyue Zhang,[†] Hongru Xu,[†] Zhenyu Wang,[†] Ying Wu,[†] Xi Shen,[†] Jiang Cui,[†] Yiu-Wing Mai,[§] and Jang-Kyo Kim^{*,†}

[†]Department of Mechanical and Aerospace Engineering, The Hong Kong University of Science and Technology, Clear Water Bay, Kowloon, Hong Kong

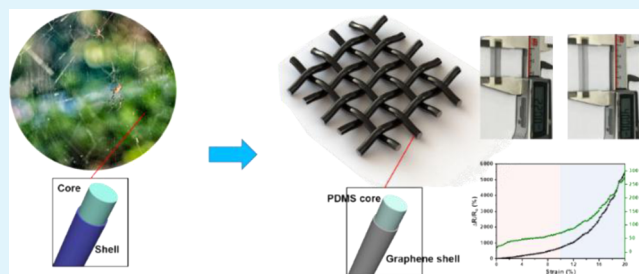
[‡]Institute for Advanced Study, The Hong Kong University of Science and Technology, Clear Water Bay, Hong Kong

[§]Centre for Advanced Materials Technology, School of Aerospace, Mechanical & Mechatronic Engineering, The University of Sydney, Sydney, NSW 2006, Australia

Supporting Information

ABSTRACT: Advanced wearable strain sensors with high sensitivity and stretchability are an essential component of flexible and soft electronic devices. Conventional metal- and semiconductor-based strain sensors are rigid, fragile, and opaque, restricting their applications in wearable electronics. Graphene-based percolative structures possess high flexibility and transparency but lack high sensitivity and stretchability. Inspired by the highly flexible spider web architecture, we propose semitransparent, ultrasensitive, and wearable strain sensors made from an elastomer-filled graphene woven fabric (E-GWF) for monitoring human physiological signals. The highly flexible elastomer microstructure and the hierarchical structure of a graphene tube offer the strain sensor with both excellent sensing and switching capabilities. Two different types of E-GWF sensors, including freestanding E-GWF and E-GWF/polydimethylsiloxane (PDMS) composites, are developed. When their structure is controlled and optimized, the E-GWF strain sensors simultaneously exhibit extraordinary characteristics, such as a high gauge factor (70 at 10% strain, which ascends to 282 at 20%) in respect to other semitransparent or transparent strain sensors, a broad sensing range up to 30%, and excellent linearity. The E-GWF/PDMS composite sensor shows a unique reversible switching behavior at a high strain level of 30–50%, making it a suitable material for fast and reversible strain switching required in many early warning systems. With a view to real-world applications of these sensors and switches, we demonstrate human motion detection and switch controls of light-emitting-diode lamps and liquid-crystal-display circuits. Their unique structure and capabilities can find a wide range of practical applications, such as health monitoring, medical diagnosis, early warning systems for structural failure, and wearable displays.

KEYWORDS: strain sensor, spider web, graphene woven fabric, stretchable, transparent



INTRODUCTION

Wearable flexible devices, especially strain sensors, have attracted growing attention for their potential applications in many fields, such as human health monitoring,^{1–4} energy storage,^{5,6} human–machine interfaces,⁷ and environmental detection.^{8,9} To achieve wearable strain sensors with overall performance suitable for practical utility, significant efforts have been devoted to developing new materials and structures. Many different materials, including metal nanoparticles and nanowires,¹⁰ conductive polymers,¹¹ graphite,¹² carbon black,¹³ carbon nanotubes,^{14–16} graphene,^{1–4,17–26} and their hybrid materials,^{8,26,27} have been used to fabricate wearable strain sensors with varied successes. Among them, graphene stands out as one of the most promising materials for next-generation wearable and sensitive strain sensors^{28,29} because it possesses many excellent properties, such as atomic layer

thickness, high electrical conductivities, high transparency, and exceptional mechanical properties.

The sensitivity of graphene-based strain sensors has been greatly improved by taking advantage of new mechanisms, including disconnection between overlapped components, crack propagation, and tunneling effect.⁴ Moreover, the stretchability, linearity, and hysteresis have also been ameliorated using new materials or new structural design.^{22,29} Despite the significant progress, simultaneous achievement of both ultrahigh sensitivity and stretchability remains a great challenge for graphene-based strain sensors. For example, although many different structures have been built using the solution-processed graphene precursor, including one-dimen-

Received: October 19, 2018

Accepted: December 24, 2018

Published: December 24, 2018

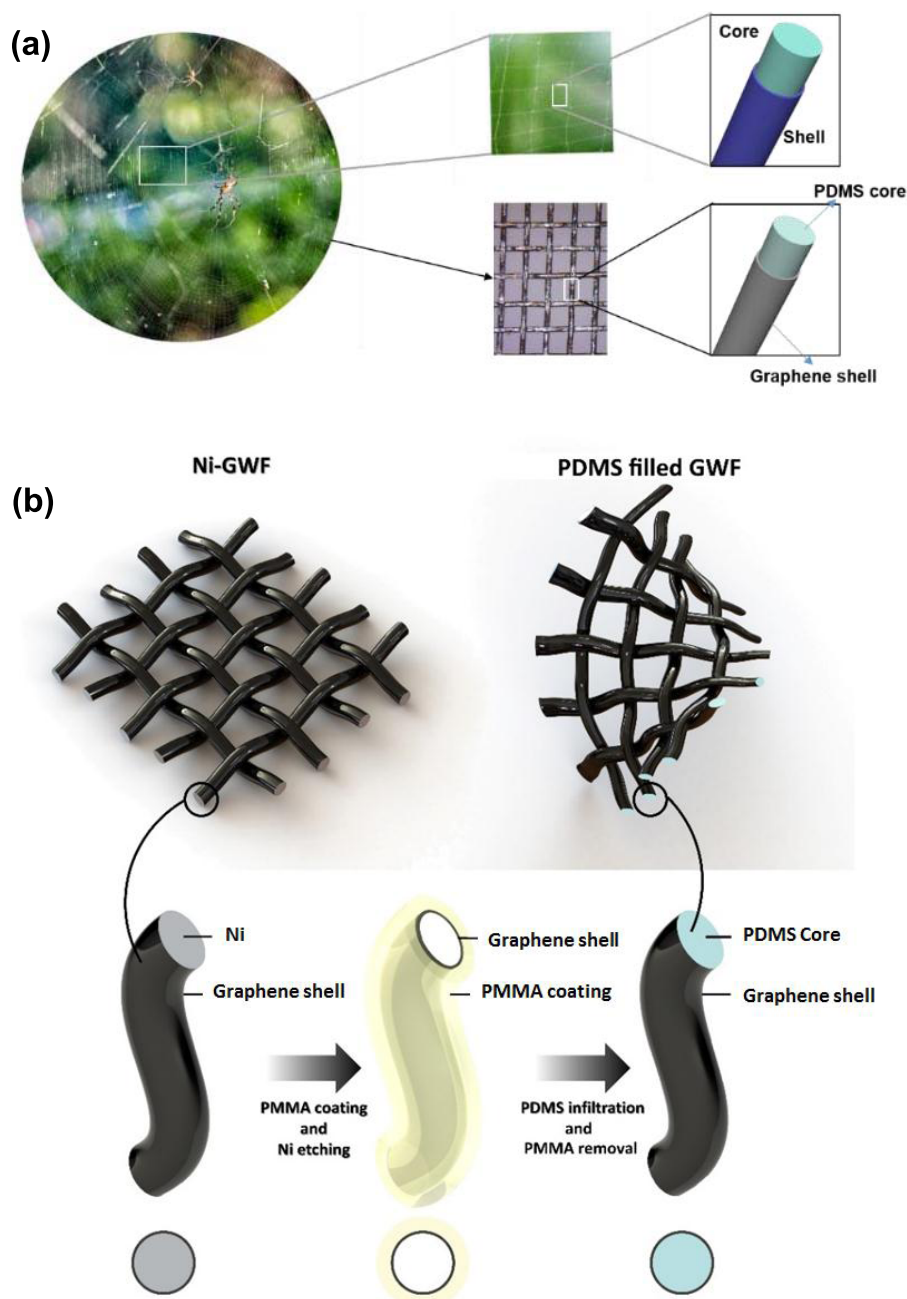


Figure 1. (a) Illustration of the concept of a spider-web-inspired elastomer-filled graphene woven fabric (E-GWF). (b) Schematic flowchart of the fabrication procedure of an E-GWF.

sional fibers,^{20,30} two-dimensional (2D) films fabricated with flakes,^{17,18} platelets,³¹ ripples,³² wrinkles,^{33,34} three-dimensional (3D) aerogels,^{35–37} and foams,³⁸ the solution process involves sophisticated chemical treatments, inevitably introducing a large number of defects in graphene. Conversely, graphene can be directly synthesized using a bottom-up strategy like chemical vapor deposition (CVD), which is scalable for manufacturing high-quality graphene while avoiding defects induced by complex solution methods. Single-layer graphene,³⁹ nano-graphene,^{23,28} graphene foams,^{21,40} graphene microtube piping,⁴¹ 3D graphene meshes,⁴² and graphene woven fabrics (GWFs)⁴³ have been synthesized by CVD for fabricating strain sensors. Because of the high-density cracks and successive cracking under strain, the GWF architecture displayed the highest sensitivity among

all graphene-based sensors. However, freestanding GWFs have low stretchability and are brittle owing to their microscale hollow structure after removing the metal template.⁴⁴ Even after combining the freestanding GWF with a flexible polymer like polydimethylsiloxane (PDMS), the stretchability of GWF/PDMS composites is still very low, usually less than 7%. Besides, the relative resistance changes of GWF/PDMS composite sensors showed a highly nonlinear relationship with the applied strain.⁴⁵ To boost the application of GWF architecture for strain sensing, it is imperative to improve the stretchability and linearity.

Materials in nature often give us important inspirations for innovative and rational design of new materials and structures. Owing to millions of years of evolution, biomaterials, such as spider silk, nacre, lotus leaf, and lobster cuticle, possess

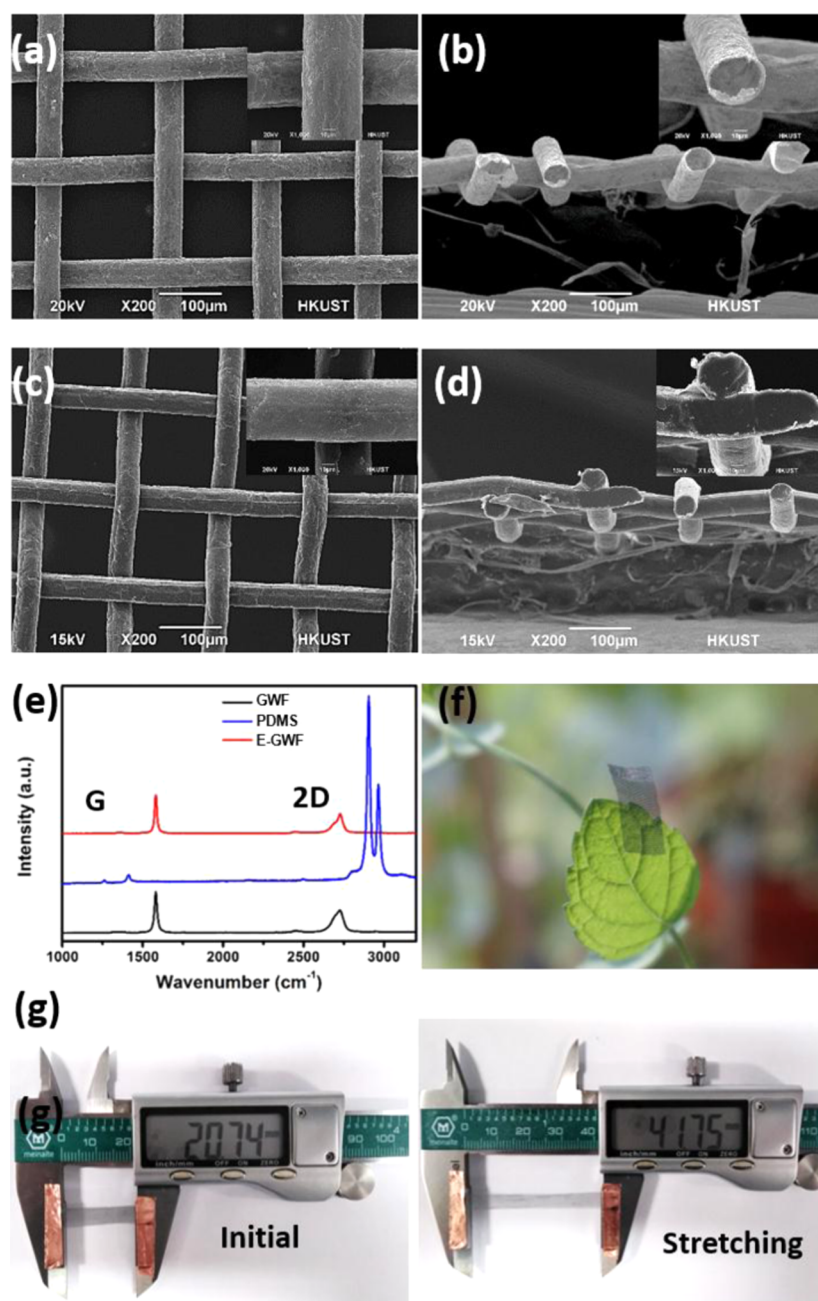


Figure 2. Characteristics of the freestanding GWF and E-GWF. Scanning electron microscope (SEM) images of (a) surface and (b) cross section of the freestanding GWF with hollow GTs. (c) Surface and (d) cross section of the freestanding E-GWF with PDMS-filled GTs. (e) Raman spectra of the freestanding GWF, pure PDMS, and E-GWF. Optical images of the freestanding E-GWF (f) on a leaf and (g) under stretching to a maximum strain of more than 100%.

amazing properties largely resulting from their sophisticated hierarchical structures.⁴⁶ Many of these structures comprise hard and soft phase materials arranged in their complex hierarchical architectures.⁴⁷ By doing so, natural organisms have both high strength and high toughness simultaneously, which are usually mutually exclusive in human-made materials. For example, strong artificial materials are usually brittle, whereas tough materials are often too weak to use for engineering applications.⁴⁸ A spider web is a remarkable example of biomaterials that combine strength with toughness, making it stretchable to a 60% tensile strain.^{49–51} As depicted in Figure 1a, the spider web is built with spider silk whose structure consists of a bundle of silk fibrils, known as spidroin,

which are encapsulated by about 100–200 nm thick outer layers made up by lipids, glyco, and skin.⁵¹ The core is 2–3 μm thick and dominates the tensile strength and elasticity. The molecular structure of silk consists of regions of protein crystals separated by less-organized protein chains. The primary structural modules give rise to diverse secondary structures that, in turn, determine the functions of different silks.⁵² Crystalline β -sheets, as one of the most extensively studied secondary structures of silks, contribute to the high tensile strength of silk fibers, whereas the noncrystalline regions of silk provide silk with elasticity. The hierarchical structure of spider silk with combined crystalline and noncrystalline regions is responsible for its super performance.

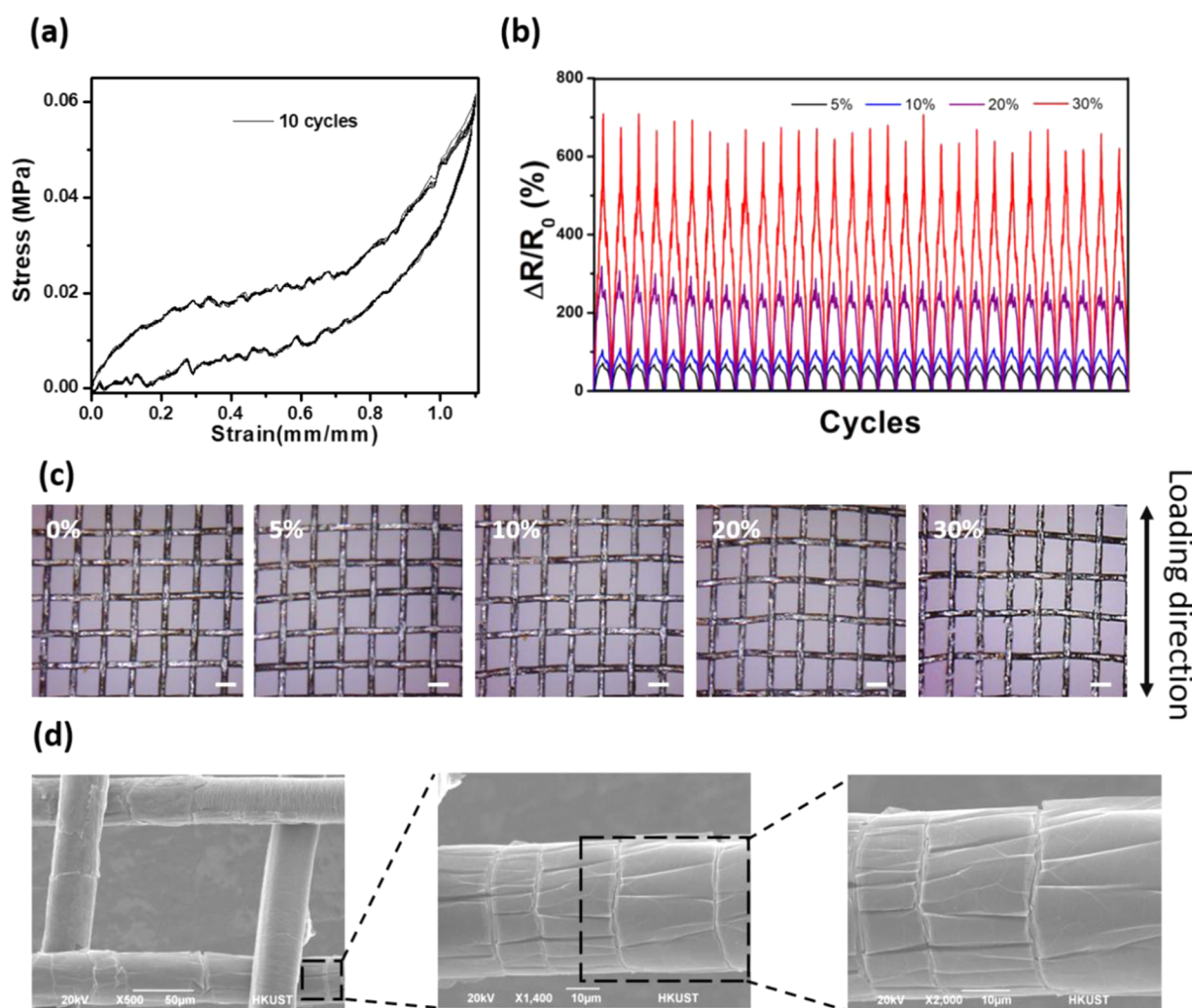


Figure 3. Characteristics of the freestanding E-GWF sensor. (a) Stress–strain curves under tensile cycles of 0–110% strain. (b) Normalized resistance changes at maximum strains of 5, 10, 20, and 30% for 30 cycles. (c) Optical images taken at different maximum strains. (d) Magnified SEM images taken at 20% tensile strain.

It is demonstrated that the superior properties of spider web stem intrinsically from the synergistic cooperation of hierarchically organized components and the web is a highly adapted system where both material and hierarchical structure across all length scales are important for its functions.⁴⁹ The GWF with weakly interconnected, hollow graphene tubes (GTs) is inherently brittle and shows low stretchability. Thus, mimicking the architecture of a spider web is a viable approach to improve its stretchability, which is an essential characteristic of wearable strain sensors.

Inspired by the unique architecture of a spider web with extraordinary stretchability, we herein propose a novel design for highly flexible and sensitive piezoresistive sensors based on an elastomer-filled graphene woven fabric (E-GWF) structure. The E-GWF also shows unusual switching behavior at large strains owing to the reversible cracking and reconnection of interconnected GTs. Figure 1b presents a schematic illustration of the E-GWF architecture that mimics the geometric and functional characteristics of a spider web. It was proposed previously⁵⁰ that there are three critical components that need to be considered when designing new functional materials, including the chemical composition, nano/microstructure, and architecture. The design of E-GWF

involves using graphene/PDMS as the main constituent to ensure high flexibility, nanoscale graphene/PDMS microfibers as the nano- and microstructural framework to provide high sensitivity, and woven fabric as the assembled architecture to guarantee structural integrity. These three components make E-GWFs an ideal bioinspired hierarchical material for strain sensors arising from the multiscale structures spanning from woven fabric, PDMS microfiber to nanoscale graphene.

RESULTS AND DISCUSSION

The microstructure of a typical CVD-grown GWF is shown in Figure 2a,b. The freestanding GWFs maintained orthogonally interconnected hollow GTs after the removal of a Ni woven fabric template, revealing a firm mesh structure of Ni woven fabric configuration. Figure 2c,d shows the surface and cross section of an E-GWF. The planar structure of GWFs with a tubular graphene assembly remained intact after the infiltration of PDMS rubber, which fully filled the hollow GTs in both the orthogonal directions. The Raman spectra of the GWF and E-GWF (Figure 2e) present two prominent peaks, namely, G and 2D band peaks associated with crystal sp^2 carbon, at ~ 1580 and ~ 2700 cm^{-1} , respectively. There was a negligible D band peak at ~ 1350 cm^{-1} related to defects or doping,

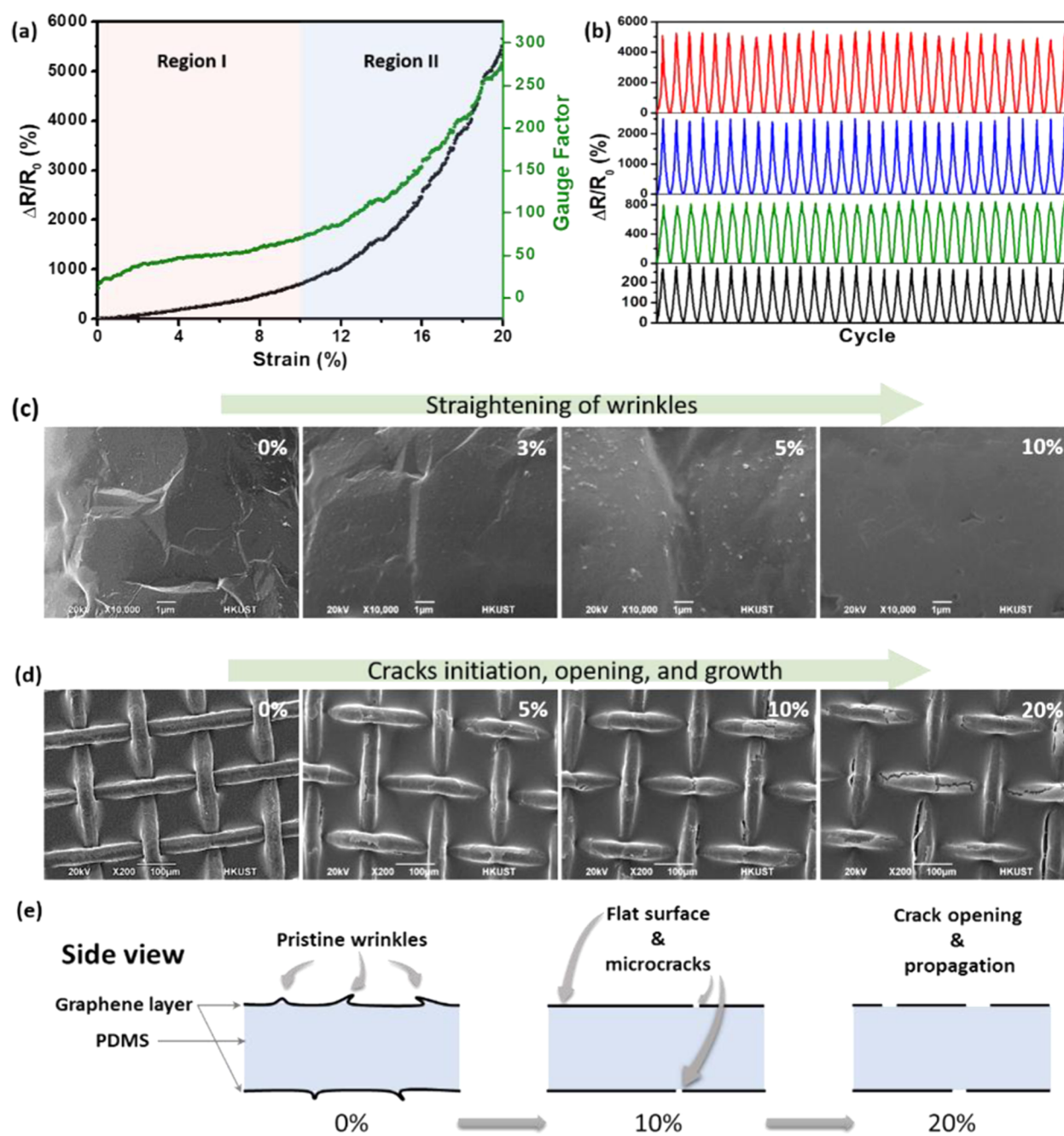


Figure 4. Characteristics of an E-GWF/PDMS sensor. (a) Normalized resistance change, $\Delta R/R_0$, and gauge factor plotted as a function of tensile strain. (b) Normalized resistance change, $\Delta R/R_0$, measured at maximum strains of 5% (black), 10% (green), 15% (blue), and 20% (red) for 30 cycles. (c) Magnified SEM images taken at 0, 3, 5, and 10% strains. (d) SEM images taken at 0, 5, 10, and 20% strains. (e) Schematic illustration of the sensing mechanisms of a composite sensor under tensile strain.

demonstrating a high quality of CVD-grown graphene.^{53,54} The Raman spectrum of pure PDMS had four characteristic peaks at ~ 1260 , ~ 1410 , ~ 2906 , and ~ 2966 cm^{-1} representing the $-\text{CH}_3$ groups. However, all of these peaks were absent in E-GWFs, indicating the PDMS core being fully covered by graphene. This also means that the structure of GWFs remained very stable during the process of infiltrating PDMS and removing the protective poly(methyl methacrylate) (PMMA) layer. It should be noted that a high methane concentration of 10 vol % was required for the growth of thick GTs, which were essential to the structural stability of the E-GWF structure. The E-GWF strip was highly flexible and

ultralight with a low density of ~ 0.08 g/cm^3 (the density is calculated by considering the rectangular strip of E-GWF with square openings), thanks to its unique fabric structure and low densities of both PDMS and graphene; see Figure 2f and Supporting Information, Video S1. More importantly, it possessed an extremely high tensile elongation of 110% (Figures 2g and 3a, Supporting Information, Videos S2 and S3). Figure 3a shows the stress–strain response of an E-GWF under 10 stretching/unloading cycles, presenting excellent reversibility with negligible hysteresis of the E-GWF sensor. In contrast, the freestanding GWF without a PDMS core

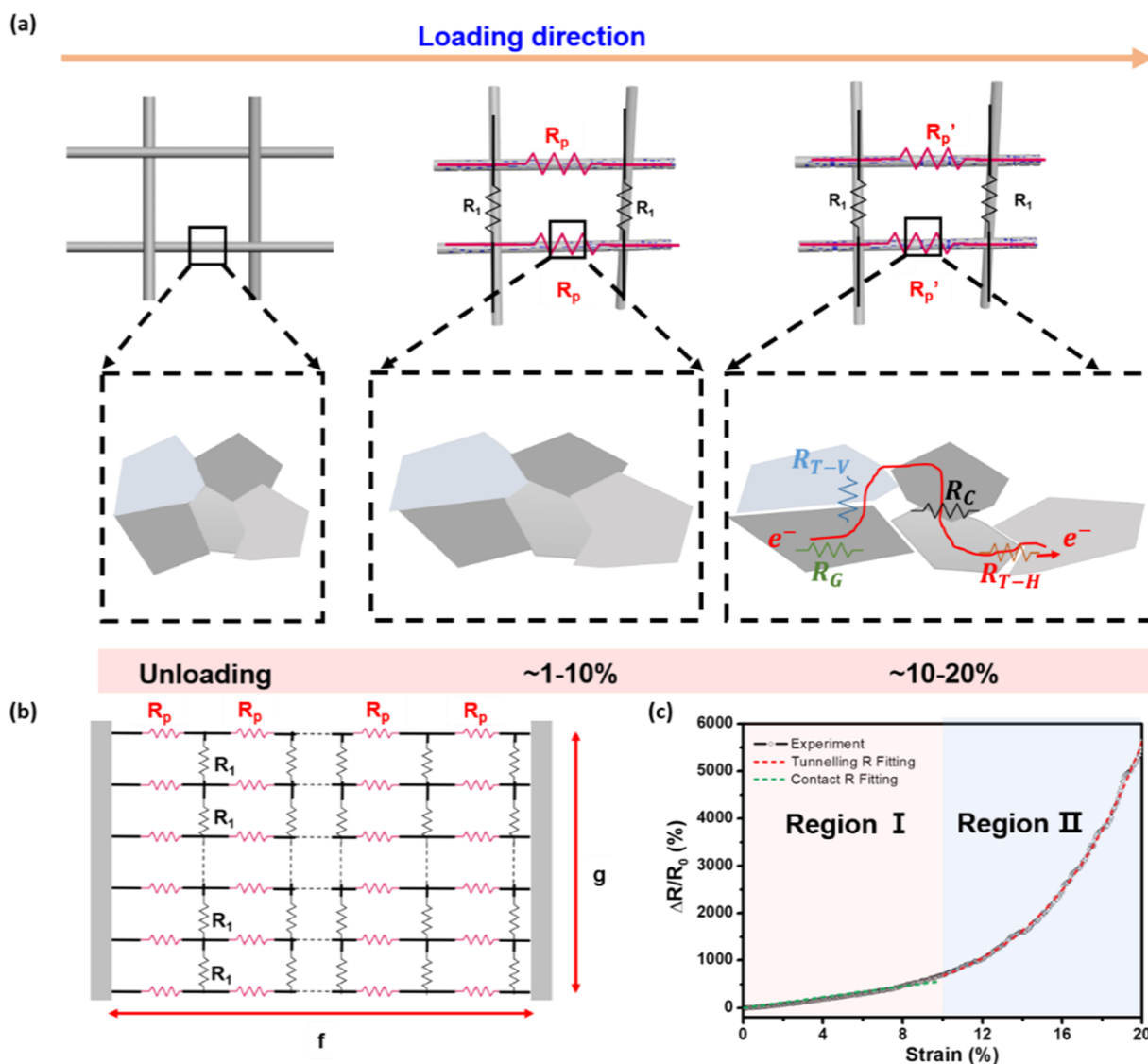


Figure 5. (a) Single equivalent circuit representing a GT unit under different tensile strains, and the schematic diagram for sliding and the forming of microcracks among graphene sheets. (b) Equivalent circuit of E-GWF structure. (c) Fitting of the experimental curve of an E-GWF/PDMS strain sensor by the contact model (region I) and the tunneling model (region II).

fractured under less than 5% tensile strain (Supporting Information, Video S4).

The sensing behavior of freestanding E-GWF strain sensors is first studied by monitoring the normalized resistance changes, $\Delta R/R_0$, at different maximum strains up to 30% for 30 cycles (Figure 3b). They displayed a monotonic increase in normalized resistance change with fairly uniform maximum changes for all strains studied. The high stretchability of freestanding films is attributed to both the unique geometric interwoven configuration (Figures 3c and S1) and the enhanced elongation of GTs filled with a highly stretchable PDMS core. The gauge factors (GFs) were ~ 15 at 5% strain and ~ 23 at 30% strain, which are about 10 times those of conventional metal-based strain gauges with a GF of ~ 2 .⁵⁵ The extraordinary capability of the freestanding E-GWF strain sensors can be attributed to their unique core-shell structure and the strong bond between the graphene shell and PDMS core. When an external strain was applied to the sensor, the graphene shell gradually fractured into pieces, exposing the inner PDMS core to the exterior. The cracked graphene shell

can be stably reconnected upon releasing the strain. Figure 3d depicts the initiation of many microcracks and their growth transverse to the tube direction with increasing applied strain. In addition to these major microcracks, wrinkles were formed along the tube direction because of the transverse shrinkage of the PDMS core⁵⁶ upon tensile loading, proving that GTs were tightly connected with the PDMS core. In contrast, little deformation, not cracking, occurred in the GTs located transverse to the loading direction, where the surface morphology remained unchanged regardless of the strain level. In view of the outstanding sensing range and the extremely high flexibility, the freestanding E-GWF sensors are ideally suited for monitoring a variety of human body motions.

To enhance the linearity, sensitivity, and structural stability, the freestanding E-GWF was embedded in a PDMS matrix forming an E-GWF/PDMS composite strain sensor. The same approach to attach the graphene sensor to a flexible substrate has been demonstrated to be effective previously, such as graphene coupled with PDMS,²² natural rubber,⁵⁷ polyacrylic ester,³⁸ and polyurethane (PU).²⁰ Although other approaches

have also been reported, including the formation of wrinkles/cracks induced by prestretching,³⁴ the shrinkage of a substrate, and the construction of three-dimensional structures,⁵⁸ their sensitivities were relatively low, making them unsuitable for GWF structures. Therefore, the E-GWF was half embedded in a flexible PDMS substrate, which was chosen for its good optical transparency and high elasticity. The E-GWF was firmly bonded with the PDMS matrix, which is particularly important for efficient load transfer from the substrate to the sensory component, ensuring excellent stretchability. The interfacial bond between the GWF shell and the PDMS core was relatively well sustained even after 5000 cycles at 50% maximum strain, as shown in the SEM image (Figure S2). The strong bond was also partly proven between the E-GWF and the PDMS matrix (shown in Figure 4d). The E-GWF/PDMS composite sensors exhibited a typical switching response time of ~ 0.07 s at a tensile strain of 30% and a loading speed of 60 mm/min, as shown in Figure S3. The excellent response time is partly ascribed to the strong bond between the PDMS core and the graphene shell.

The normalized resistance changes and GFs of the E-GWF/PDMS composite sensors measured at tensile strains up to 20% are shown in Figure 4a,b. The normalized resistance monotonically increased with increasing strain and returned to the initial value upon release of the strain, verifying high repeatability under cyclic loading (Figure 4b). It is interesting to note that the relationship between the resistance change and the applied strain can be divided into two regions, region I and region II, according to the slope of the curve (Figure 4a). The E-GWF/PDMS composite sensor showed a good linear relationship between $\Delta R/R_0$ and strain up to 10% (region I) with a high coefficient of determination (R^2) of 0.9810 and a maximum GF of ~ 70 . It is noted that the freestanding E-GWF sensor showed a slightly lower R^2 value, 0.8931 (Figure S4), and a maximum GF of ~ 10 in the same strain range. In region II, the GF drastically increased to 282 at 20% strain, which is much higher than that of the freestanding E-GWF sensor.

To shed light on the mechanisms behind the exceptional GFs, the changes in surface morphology of an E-GWF/PDMS composite sensor at different strains were monitored by ex situ SEM to track the structural evolution, as shown in Figure 4c,d. The wrinkles acting as grain boundaries on GTs were gradually flattened upon stretching, and they became completely flat when the strain reached $\sim 10\%$ (Figure 4c). As the strain further increased beyond $\sim 10\%$, microcracks appeared along the flattened wrinkles and grew gradually at higher strains on the GTs running in the loading direction (Figure 4d), resulting in reduction of the contact area among the graphene layers. The cracking of GTs appears to be very similar to that of the graphene foam structure, which fractured because of the presence of defects and stress concentrations at grain boundaries.²⁹ The resistance increased rapidly as a result of cracked GTs, leading to a higher piezoresistive sensitivity (i.e., $\text{GF} > 280$) at a high strain of more than 20%. It should be noted that the aforementioned flattening of wrinkles and the formation and growth of cracks were reversible upon release of the applied strain. This signifies repeatable cracking/healing behavior with a highly durable sensing capability of the E-GWF/PDMS composite sensor. As such, different piezoresistive sensing mechanisms are proposed for region I and region II, as illustrated in Figure 4e. In region I, the increase in resistance is moderate and gradual, and is mainly attributed to straightening of wrinkles on GTs. In region II, microcracks

were initiated and grew longer and wider perpendicular to the loading direction and trenches started to emerge, leading to the interruption and rupture of conductive paths in the tubes running in the loading direction. The microscale wrinkles on GTs played an important role in broadening the strain range as well as significantly contributed to enhanced sensitivity of both E-GWF and E-GWF/PDMS sensors because they are firmly held by the stretchable PDMS core even after cracking of GTs. This observation differs from the wrinkles in flat graphene sheets induced by prestretching or shrinkage, which showed almost no obvious resistance changes under strain.⁵⁹

To further analyze the sensing mechanism, an equivalent circuit model is proposed on the basis of a square GT grid of an E-GWF sensor under strain, as shown in Figure 5a. The GTs consisted of polycrystalline graphene sheets connected by a number of grain boundaries. In light of microscopic observations (Figures 3d and 4c,d) and schematic sensory mechanism (Figure 4e), the boundaries between the adjacent graphene sheets were defined depending on the applied strain: namely, (i) solid contact with changes in contact area due to flattening of wrinkles and relative sliding and (ii) tunneling junction due to crack initiation and growth. When the applied strain increases, the dominant source of resistance change gradually shifts from the change in contact area to tunneling distance, and the critical strain is $\sim 10\%$ according to the piezoresistive behavior of the sensor.

R_p and R_p' represent the resistances of GTs paralleled to the loading direction at low and high strains, respectively, whereas R_1 is the resistance of a GT perpendicular to the loading direction, which is assumed to be constant because of negligible structural changes by stretching (Figure 5a). In light of the microstructural change under a tensile strain leading to microcracking (Figures 3d and 4e), the resistance R_p can be divided into four components, including the intrinsic resistance of graphene (R_{N1}), the contact resistance among the overlapped graphene sheets (R_{N2}), the tunneling resistance induced by horizontal microcracks (R_{N3}), and the tunneling resistance induced by vertical microcracks (R_{N4})

$$R_p = pR_{N1} + qR_{N2} + rR_{N3} + sR_{N4} \quad (1)$$

where p , q , r , and s are the total number of R_{N1} , R_{N2} , R_{N3} , and R_{N4} encountered. The E-GWF structure consists of many interconnected rectangular units (Figure 5b); thus, a simple equivalent circuit model is built by assuming that all of the parallel GTs have the same resistance. Then, the total resistance is given by⁶⁰

$$R_{\text{total}} = \frac{f}{g}(R_p + R_1) \quad (2)$$

where the ratio, f/g , represents the ratio of resistor numbers parallel to transverse to the loading direction (Figure 5b). In region I, the change in contact resistance R_{N2} dominates the resistance behavior because sliding occurs among the graphene layers without any cracking. Then, $\Delta R/R_0$ can be calculated by (with the details given in the Supporting Information, eqs S1–S5)

$$\frac{\Delta R}{R_0} = k\varepsilon \quad (3)$$

where k is the strain-independent parameter of the overlapped area and ε is the applied tensile strain. The proposed contact model given by eq 3 fits well the experimental curve in region I,

showing a linear relationship between the resistivity and the tensile strain (Figure 5c). In region II, the change in tunneling resistance, R_{N3} , dominates the resistance where R_{N3} is much larger than R_{N4} and the change in R_{N4} can be ignored. Thus, the total resistance change, $\Delta R/R_0$, can be written by (with the details given in the Supporting Information, eqs S6–S13)⁶¹

$$\frac{\Delta R}{R_0} = (1 + k''\epsilon)(1 + k'\epsilon)\exp\left(\frac{4\pi w_0 k'' \sqrt{2m\phi}}{h}\right) - 1 \quad (4)$$

where k'' is the strain-independent parameter of the tunneling distance, k' is the strain-independent parameter of the conduction area, m is the electron mass, ϕ is the potential height from the Fermi level, h is Planck's constant, and w_0 is the original tunneling distance. The relationship between the relative resistance change and the structural change associated with microcrack initiation and growth can be reasonably explained by the tunneling model, eq 4, which fits well the experimental curve (Figure 5c).

The normalized resistance changes measured for 30, 200, and 4000 cycles (Figures 4b, S5a–d, and S6a, respectively) clearly demonstrate the highly repeatable stretchability and durability of the composite sensors over a very wide range of strains. Attributed to the strong interfacial bond between the GWF and the PDMS core as well as between the E-GWF and the PDMS substrate, the sensors exhibited a uniform and fully recoverable electrical resistance with negligible stress–strain hysteresis (Figure S7). In addition, the composite sensors present an excellent balance between the sensitivity and the sensing range. The gauge factors and maximum sensing strains of various strain sensors fabricated with CVD-grown graphene are compared in Figure 6a. High sensitivity was achieved using planar graphene structures with interconnected conductive networks, whereas high stretchability was obtained using high-quality graphene layers. However, these sensors failed to have both high sensitivity and high stretchability simultaneously. The comparison clearly indicates that the E-GWF/PDMS composite sensor possessed a balanced combination of high sensitivity and high stretchability, thanks to the presence of both high-quality GTs and PDMS core. Furthermore, the E-GWF/PDMS sensor was semitransparent with a transparency of $\sim 47\%$ for a range of visible-light wavelengths and the transparency slightly increased upon stretching because of the increase in the number of cracks (Figures S8 and S9). This characteristic may be particularly attractive for skin-mountable strain sensors.

More interestingly, when the tensile strain was varied between 30 and 50%, its resistance instantaneously surged by 6–8 orders of magnitude, i.e., from ~ 1 k Ω to more than 200 M Ω (Figure 6b), showing a fascinating reversible on/off switching behavior. Furthermore, the resistance spontaneously recovered upon releasing the strain below the critical switching strain of $\sim 30\%$. This means that the E-GWF/PDMS composite switch offers an extremely high sensitivity, 10^3 – 10^4 times higher than that of previously developed graphene or CNT-based switching devices.^{62,63}

Extremely high sensitivity is also observed in other types of strain sensors such as cracking (silver ink patterned silicone elastomer)-(silver-plated nylon structure) (Ag-DS/CF) and polyurethane (PU)-foam films,^{64,65} which showed $\Delta R/R_0$ of approximately 5×10^{11} . Similarly, it can be inferred that the exciting switching behavior of the E-GWF/PDMS composite switch is also attributed to the tunneling effect between the

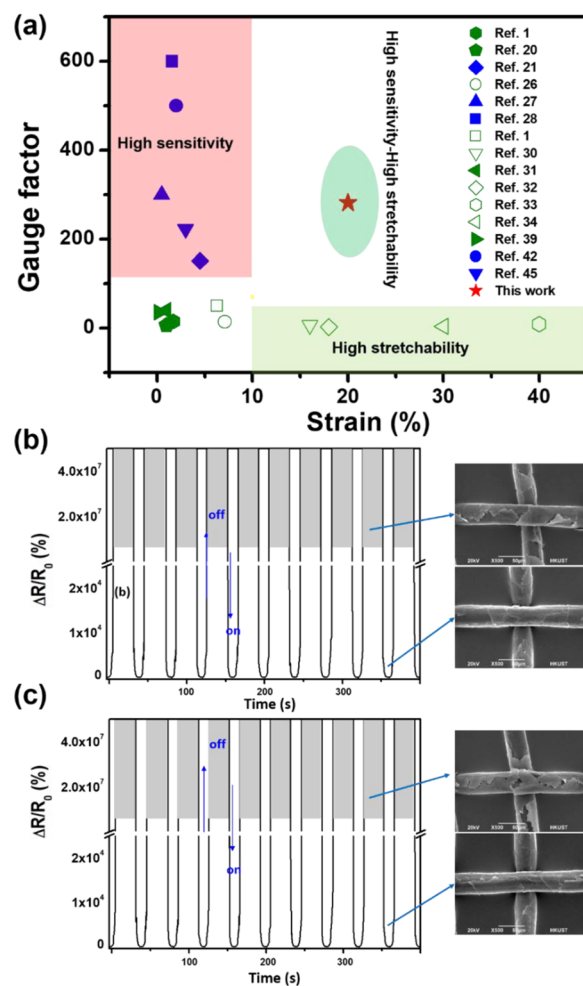


Figure 6. (a) Comparison of gauge factors and maximum sensing strains of various strain sensors fabricated with CVD-grown graphene reported in the literature. Cyclic switching performance of an E-GWF/PDMS strain sensor at strains of (b) 30% and (c) 50%. The corresponding SEM images of GTs taken under load and after unloading.

cracked graphene shell and the PDMS core. It can be seen that many trenches emerged and the GTs were transformed into many fragments (Figure 6c) when a large number of microcracks were generated transverse to the tube direction and between the graphene–graphene interface at a high strain, whereas the PDMS core remained intact to continuously hold the graphene layers. Then, a surge in electrical resistance ensued. Upon release of the applied strain, the graphene fragments fully recovered to their original state along with recovery of conductive networks. The good adhesion between the PDMS microskeleton and graphene layers and the stretchability of PDMS ensured the highly reversible electrical interconnection and disconnection under repeated loading cycles. Beyond the switching range above 50% strain, some cracked graphene layers were detached from the PDMS core, resulting in an irreversible structural change. This finding signifies that the flexible PDMS applied as the core of GTs played an important role to offer the E-GWF/PDMS composite with a reversible switching capability and the necessary long-term structural durability in the range of 30–50% strain. The switching response was not only very fast but also highly reversible for many stretching and releasing cycles.

Even after 200 switching cycles, the E-GWF/PDMS composite retained a good conductivity at a low strain level below 20% and maintained an extremely high resistivity at a high strain level above 30% (Figure S3e,f). Microcracks gradually formed upon initial several cycles, and the performance of the sensor became stable and almost fully reversible with further increasing cycles at strains below 50%. The E-GWF/PDMS strain sensor presented high durability for more than 4000 cycles at different strains of 5 and 50% (Figure S6), demonstrating both excellent sensing and switching capabilities. The typical initial resistance of E-GWF/PDMS was in the range of 1–10 k Ω , which could be further reduced via several strategies, including the improved quality of graphene sheets, increased number of graphene layers, and doping treatment.

Taking advantage of the aforementioned outstanding sensitivity, excellent flexibility, broad working range, and unique switching behavior, we demonstrated the applications of E-GWF-based strain sensors/switches for human motion detection and wearable displays, as shown in Figure 7a–f. The freestanding E-GWF sensor was able to detect and distinguish the motions of finger (Figure 7a,b) and neck (Figure 7b,c). In addition to monitoring the large human motions, the E-GWF/PDMS composite sensor was applied to detect very subtle motions, such as phonation and music. The different physiological reactions caused by throat were distinguished by the peak pattern and intensity, as shown in Figure 7e,f. The composite sensor was attached to the surface of a common mobile-phone loudspeaker (Figure 7g). It is noted that different music alphabet letters were accurately distinguished by different peak patterns, confirming the sensor's extremely high sensitivity and fast response (Figure 7h–k). Besides, the sensor can also be used to differentiate pronunciations for both English and Chinese, which shows a great potential for many new applications related to speech recognition (Figure S10).

In addition, three circuits were specially designed to illustrate the sensing and on/off switching capabilities of the composite sensor and thus to demonstrate its potential for wearable displays. In the circuits, the “on” state is equivalent to a low resistance change at a low strain, whereas the “off” state corresponds to a strain higher than the threshold of 30% with an extremely high resistance (Figure 6). In the first circuit, only one light emitting diode (LED) lamp was connected to the E-GWF/PDMS sensor, as shown in Figure S11 and Supporting Information, Video S5. The LED lamp was dimmed and completely turned off when the sensor was stretched, whereas the LED lamp was turned on with increasing brightness upon releasing the strain. In the second circuit, five LED lamps were displayed, as shown in Figure 8a and Supporting Information, Video S6. Initially, all five LED lamps were illuminated before stretching. By gradually stretching the sensor below 30% strain, the resistance gradually increased to the default threshold value, leading to turning off one by one. All LED lamps were turned off when the applied strain exceeded 30% and were turned on in sequence again upon releasing the strain at almost the identical displacements, confirming the reversibility of on/off switching functions. In the third circuit, the LED lamp was replaced by an liquid crystal display (LCD) that displayed the word “HKUST”. The characters “UST” disappeared from the display when the strain was higher than the critical switching strain during stretching and appeared upon releasing (see Figure 8b). The aforementioned findings demonstrate the switching capability of the flexible E-GWF/PDMS switch where the LED lamps were accurately switched on/off and the

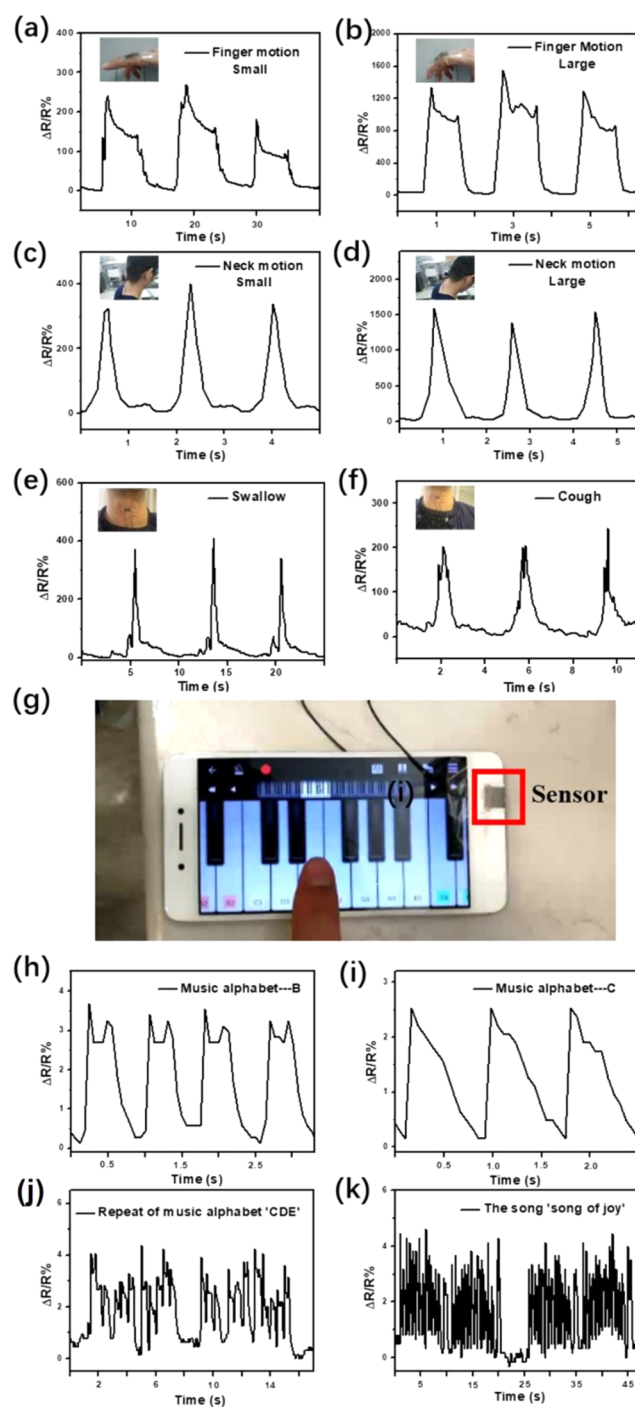


Figure 7. Applications of E-GWF-based strain sensors. Monitoring of human motions, including (a, b) finger and (c, d) neck motions, (e) swallowing, and (f) coughing. Detection of tiny vibrations induced by music with an E-GWF/PDMS strain sensor: (g) E-GWF/PDMS strain sensor attached to a mobile-phone's loudspeaker; resistance changes induced by (h) music alphabet B, (i) music alphabet C, (j) a simple repeat of the music alphabet CDE–CDE, and (k) the song “the song of joy”.

LCD output signals were precisely controlled. To exhibit the function of the E-GWF/PDMS switch in wearable devices, the sensor was mounted on a wrist (Figure 8c) and the LED lamps were displayed stably on/off by wrist bending (Supporting Information, Video S7). The on/off switching of LED lamps was made possible by the bending cycles between the angles

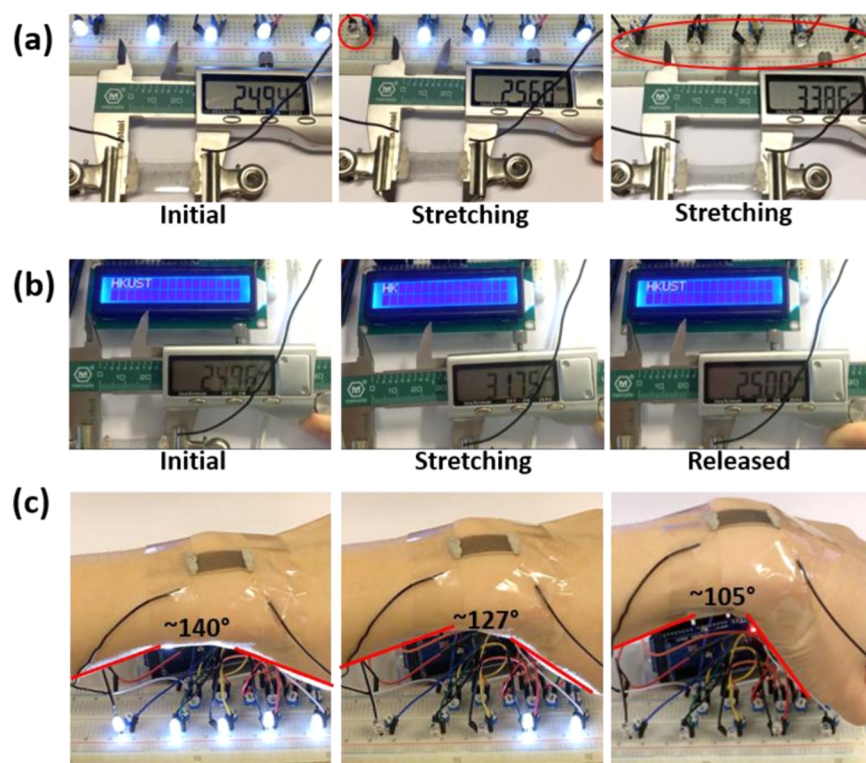


Figure 8. Applications of E-GWF/PDMS composite switches. (a) Switching on/off an LED device with cyclic stretching. (b) LCD device displaying on/off HKUST under cyclic stretching. (c) Controlling the LED lamps by wrist bending.

$\sim 140^\circ$ and $\sim 105^\circ$, where the resistance changes reached below and above the default switching threshold, respectively.

CONCLUSIONS

In summary, bioinspired spider-web-like E-GWFs were designed and synthesized by infiltrating flexible PDMS rubber into the hollow GTs in CVD-grown GWFs. E-GWF/PDMS composite sensors were assembled by bonding the E-GWFs onto the PDMS films, which delivered excellent stretchability, linearity, and stability. By carefully optimizing the structural parameters, the E-GWF/PDMS sensor simultaneously exhibited a high gauge factor of 70 at 10% strain, which increased to 282 when the strain was extended to 20%. It maintained a broad sensing range up to 30% and an excellent linearity of 0.9810 for 0–10% strains. When the applied strain was increased beyond 30%, the E-GWF/PDMS sensor displayed a unique reversible switching behavior. It is found that the repeatable reconnection of the cracked GTs covering the PDMS core skeleton after unloading gave rise to good reversibility of the sensor. The infiltrated flexible PDMS core played an important role in not only supporting the conductive networks of the GT shell and thus enhancing the sensing capability but also providing reversibility and high reliability to the stretchable device to realize long-term use under both low and high strain ranges.

Furthermore, a simple equivalent circuit model was built to explain and predict the performance of the E-GWF/PDMS sensor. It is demonstrated that the contact resistance and the tunneling resistance dominate within and beyond the initial 10% tensile strain, respectively. The wearable E-GWF/PDMS sensor was demonstrated to monitor physiological motions, including finger and neck motions, swallowing, and coughing, and distinguish tiny vibrations induced by different alphabet

letters, signifying its great potential for use in speech recognition. By means of their on/off switching capabilities, the LED and LCD circuits were accurately controlled through cyclic loading and unloading, which are particularly attractive for many emerging wearable applications, such as personal electronics, human–machine interfaces, health monitoring, and biomedical devices.

METHODS

Synthesis of E-GWF Strain Sensors. Ni meshes (200 meshes in a $25.4 \times 25.4 \text{ mm}^2$ square with $56 \mu\text{m}$ in diameter, supplied by Beijing Century Woven Corp) were cleaned, tailored, and pretreated before placing into the quartz tube of a CVD furnace.^{66,67} Pure H_2 and Ar were introduced into the furnace, and it was heated to 1000°C within 60 min, which was kept constant for 30 min. Then, the flow of H_2 was stopped and CH_4 (20 sccm) was introduced for 20 min at ambient pressure. After the CH_4 supply was stopped, the furnace was rapidly cooled to room temperature at a rate of $\sim 100^\circ\text{C}/\text{min}$. During the above processes, the flow of Ar was maintained at 200 sccm. Finally, graphene layers were deposited on the Ni mesh. The as-received Ni-GWFs were coated with 20 wt % poly(methyl methacrylate) (PMMA)/*N,N*-dimethylformide solution by dip-coating, and the solvent was evaporated in an oven at 80°C for 3 h for PMMA curing. The Ni template was removed by immersing the coated GWFs in 3 M hydrochloric acid at 80°C for 24 h to obtain GWF/PMMA films. The hollow GTs in GWF/PMMA films were filled with PDMS solution (Sylgard184, Dow Corning, base/curing agent = 10:1 by weight) under vacuum for 4 h at room temperature, followed by curing at 80°C for 2 h. The liquid PDMS solution was driven into the $56 \mu\text{m}$ thick hollow GTs by a capillary effect. The highly hydrophobic nature of the graphene surface also facilitated the infiltration. The PMMA coating was removed in hot acetone to obtain freestanding E-GWFs. Then, E-GWF/PDMS composites were prepared by embedding E-GWFs into the partially cured sticky PDMS matrix film. Finally, the composites were cut into rectangular strips and connected with

copper wires using a silver paste to form E-GWF/PDMS composite sensors.

Characterization. An optical microscope (Olympus BX51M), a scanning electron microscope (SEM, JEOL JSM-6390F), and a transmission electron microscope (TEM, JEOL 2010) were used to characterize the microstructures and morphologies of freestanding GWF, E-GWF, and E-GWF/PDMS composites. Raman spectra were recorded using a Micro-Raman spectrometer (Renishaw Micro-Raman/Photoluminescence System) with a He–Ne laser source at an excitation wavelength of 633 nm. The electromechanical characterization was performed by loading the strain sensors in tension on a universal testing machine (MTS Alliance RT-5) at a cross-head speed of 1 mm/min. The electrical resistance was continuously monitored using a digital multimeter (34970A Data Acquisition/Data Logger Switch Unit, Agilent) while the sensors were under load. A digital oscilloscope (Tektronix, TBS 1072B-EDU) was used to monitor the resistance changes of E-GWF and E-GWF/PDMS composites when attached to different parts of a human body.

■ ASSOCIATED CONTENT

Supporting Information

The Supporting Information is available free of charge on the ACS Publications website at DOI: 10.1021/acsami.8b18312.

Additional characterization of the freestanding E-GWF; cyclic performance of the E-GWF/PDMS composite sensor; transmittance spectrum of the E-GWF/PDMS composite sensor; derivation of theoretical models (PDF)

High flexibility and low density of the freestanding E-GWF (Video S1) (AVI)

Stretching of the freestanding E-GWF (Video S2) (AVI)

Stretching and bending of the freestanding E-GWF (Video S3) (AVI)

Comparison of stretchabilities between the freestanding E-GWF and GWF (Video S4) (AVI)

LED lamp circuit (Video S5) (AVI)

LED lamps under cyclic stretching (Video S6) (AVI)

Wearable sensor connected to LED lamps (Video S7) (AVI)

■ AUTHOR INFORMATION

Corresponding Authors

*E-mail: mezheng@ust.hk (Q.Z.).

*E-mail: mejkkim@ust.hk (J.-K.K.).

ORCID

Xi Shen: 0000-0003-1688-4931

Jang-Kyo Kim: 0000-0002-5390-8763

Author Contributions

^{||}X.L. and D.L. contributed equally to this work.

Author Contributions

The manuscript was written through contributions of all authors. All authors have given approval to the final version of the manuscript.

Notes

The authors declare no competing financial interest.

■ ACKNOWLEDGMENTS

This project was financially supported by the Research Grants Council of Hong Kong SAR (GRF projects: 16229216, 16209917, and 16205517) and the Initiation Grant for New Faculty (IGN15EG06). Technical assistance from the Advanced Engineering Materials facilities (AEMF) and the

Materials Characterization and Preparation Facilities (MCPF) of HKUST is appreciated.

■ REFERENCES

- (1) Wang, Y.; Wang, L.; Yang, T.; Li, X.; Zang, X.; Zhu, M.; Wang, K.; Wu, D.; Zhu, H. Wearable and Highly Sensitive Graphene Strain Sensors for Human Motion Monitoring. *Adv. Funct. Mater.* **2014**, *24*, 4666–4670.
- (2) Allen, M. J.; Tung, V. C.; Kaner, R. B. Honeycomb Carbon: a Review of Graphene. *Chem. Rev.* **2010**, *110*, 132–145.
- (3) Wang, C.; Li, X.; Gao, E.; Jian, M.; Xia, K.; Wang, Q.; Xu, Z.; Ren, T.; Zhang, Y. Carbonized Silk Fabric for Ultrastretchable, Highly Sensitive, and Wearable Strain Sensors. *Adv. Mater.* **2016**, *28*, 6640–6648.
- (4) Amjadi, M.; Kyung, K.-U.; Park, I.; Sitti, M. Stretchable, Skin-Mountable, and Wearable Strain Sensors and Their Potential Applications: a Review. *Adv. Funct. Mater.* **2016**, *26*, 1678–1698.
- (5) Chong, W. G.; Huang, J.-Q.; Xu, Z.-L.; Qin, X.; Wang, X.; Kim, J.-K. Lithium–Sulfur Battery Cable Made from Ultralight, Flexible Graphene/Carbon Nanotube/Sulfur Composite Fibers. *Adv. Funct. Mater.* **2017**, *27*, No. 1604815.
- (6) Wen, L.; Li, F.; Cheng, H. M. Carbon Nanotubes and Graphene for Flexible Electrochemical Energy Storage: from Materials to Devices. *Adv. Mater.* **2016**, *28*, 4306–4337.
- (7) Roh, E.; Hwang, B.-U.; Kim, D.; Kim, B.-Y.; Lee, N.-E. Stretchable, Transparent, Ultrasensitive, and Patchable Strain Sensor for Human–Machine Interfaces Comprising a Nanohybrid of Carbon Nanotubes and Conductive Elastomers. *ACS Nano* **2015**, *9*, 6252–6261.
- (8) Yang, J.; Wei, D.; Tang, L.; Song, X.; Luo, W.; Chu, J.; Gao, T.; Shi, H.; Du, C. Wearable Temperature Sensor Based on Graphene Nanowalls. *RSC Adv.* **2015**, *5*, 25609–25615.
- (9) Huang, G.-W.; Xiao, H.-M.; Fu, S.-Y. Electrical Switch for Smart pH Self-Adjusting System Based on Silver Nanowire/Polyaniline Nanocomposite Film. *ACS Nano* **2015**, *9*, 3234–3242.
- (10) Liao, X.; Zhang, Z.; Kang, Z.; Gao, F.; Liao, Q.; Zhang, Y. Ultrasensitive and Stretchable Resistive Strain Sensors Designed for Wearable Electronics. *Mater. Horiz.* **2017**, *4*, 502–510.
- (11) Wang, T.; Zhang, Y.; Liu, Q.; Cheng, W.; Wang, X.; Pan, L.; Xu, B.; Xu, H. A Self-Healable, Highly Stretchable, and Solution Processable Conductive Polymer Composite for Ultrasensitive Strain and Pressure Sensing. *Adv. Funct. Mater.* **2018**, *28*, No. 1705551.
- (12) Liao, X.; Liao, Q.; Yan, X.; Liang, Q.; Si, H.; Li, M.; Wu, H.; Cao, S.; Zhang, Y. Flexible and Highly Sensitive Strain Sensors Fabricated by Pencil Drawn for Wearable Monitor. *Adv. Funct. Mater.* **2015**, *25*, 2395–2401.
- (13) Song, H.; Zhang, J.; Chen, D.; Wang, K.; Niu, S.; Han, Z.; Ren, L. Superfast and High-sensitivity Printable Strain Sensors with Bioinspired Micron-scale Cracks. *Nanoscale* **2017**, *9*, 1166–1173.
- (14) Yamada, T.; Hayamizu, Y.; Yamamoto, Y.; Yomogida, Y.; Izadi-Najafabadi, A.; Futaba, D. N.; Hata, K. A Stretchable Carbon Nanotube Strain Sensor for Human-Motion Detection. *Nat. Nanotechnol.* **2011**, *6*, 296–301.
- (15) Lipomi, D. J.; Vosgueritchian, M.; Tee, B. C.; Hellstrom, S. L.; Lee, J. A.; Fox, C. H.; Bao, Z. Skin-like Pressure and Strain Sensors Based on Transparent Elastic Films of Carbon Nanotubes. *Nat. Nanotechnol.* **2011**, *6*, 788–792.
- (16) Liu, Z.; Qi, D.; Guo, P.; Liu, Y.; Zhu, B.; Yang, H.; Liu, Y.; Li, B.; Zhang, C.; Yu, J.; Liedberg, B.; Chen, X. Thickness-Gradient Films for High Gauge Factor Stretchable Strain Sensors. *Adv. Mater.* **2015**, *27*, 6230–6237.
- (17) Boland, C. S.; Khan, U.; Backes, C.; O'Neill, A.; McCauley, J.; Duane, S.; Shanker, R.; Liu, Y.; Jurewicz, I.; Dalton, A. B.; Coleman, J. Sensitive, High-Strain, High-Rate Bodily Motion Sensors Based on Graphene–Rubber Composites. *ACS Nano* **2014**, *8*, 8819–8830.
- (18) Hempel, M.; Nezich, D.; Kong, J.; Hofmann, M. A Novel Class of Strain Gauges Based on Layered Percolative Films of 2D Materials. *Nano Lett.* **2012**, *12*, 5714–5718.

- (19) Zhao, J.; Wang, G.; Yang, R.; Lu, X.; Cheng, M.; He, C.; Xie, G.; Meng, J.; Shi, D.; Zhang, G. Tunable Piezoresistivity of Nanographene Films for Strain Sensing. *ACS Nano* **2015**, *9*, 1622–1629.
- (20) Cheng, Y.; Wang, R.; Sun, J.; Gao, L. A Stretchable and Highly Sensitive Graphene-Based Fiber for Sensing Tensile Strain, Bending, and Torsion. *Adv. Mater.* **2015**, *27*, 7365–7371.
- (21) Jeong, Y. R.; Park, H.; Jin, S. W.; Hong, S. Y.; Lee, S.-S.; Ha, J. S. Highly Stretchable and Sensitive Strain Sensors Using Fragmentized Graphene Foam. *Adv. Funct. Mater.* **2015**, *25*, 4228–4236.
- (22) Liu, X.; Tang, C.; Du, X.; Xiong, S.; Xi, S.; Liu, Y.; Shen, X.; Zheng, Q.; Wang, Z.; Wu, Y.; Horner, A.; Kim, J.-K. A Highly Sensitive Graphene Woven Fabric Strain Sensor for Wearable Wireless Musical Instruments. *Mater. Horiz.* **2017**, *4*, 477–486.
- (23) Lee, Y.; Bae, S.; Jang, H.; Jang, S.; Zhu, S. E.; Sim, S. H.; Song, Y. I.; Hong, B. H.; Ahn, J. H. Wafer-Scale Synthesis and Transfer of Graphene Films. *Nano Lett.* **2010**, *10*, 490–493.
- (24) Bae, S.-H.; Lee, Y.; Sharma, B. K.; Lee, H.-J.; Kim, J.-H.; Ahn, J.-H. Graphene-Based Transparent Strain Sensor. *Carbon* **2013**, *51*, 236–242.
- (25) Wang, X.; Qiu, Y.; Cao, W.; Hu, P. Highly Stretchable and Conductive Core–Sheath Chemical Vapor Deposition Graphene Fibers and Their Applications in Safe Strain Sensors. *Chem. Mater.* **2015**, *27*, 6969–6975.
- (26) Zhang, H.; Liu, N.; Shi, Y.; Liu, W.; Yue, Y.; Wang, S.; Ma, Y.; Wen, L.; Li, L.; Long, F.; Zou, Z.; Gao, Y. Piezoresistive Sensor with High Elasticity Based on 3D Hybrid Network of Sponge@CNTs@Ag NPs. *ACS Appl. Mater. Interfaces* **2016**, *8*, 22374–22381.
- (27) Yan, C.; Wang, J.; Kang, W.; Cui, M.; Wang, X.; Foo, C. Y.; Chee, K. J.; Lee, P. S. Highly Stretchable Piezoresistive Graphene–Nanocellulose Nanopaper for Strain Sensors. *Adv. Mater.* **2014**, *26*, 2022–2027.
- (28) Zhao, J.; He, C.; Yang, R.; Shi, Z.; Cheng, M.; Yang, W.; Xie, G.; Wang, D.; Shi, D.; Zhang, G. Ultra-Sensitive Strain Sensors Based on Piezoresistive Nanographene Films. *Appl. Phys. Lett.* **2012**, *101*, No. 063112.
- (29) Zheng, Q.; Liu, X.; Xu, H.; Cheung, M.-S.; Choi, Y.-W.; Huang, H.-C.; Lei, H.-Y.; Shen, X.; Wang, Z.; Wu, Y.; Kim, S.-Y.; Kim, J.-K. Sliced Graphene Foam Films for Dual-Functional Wearable Strain Sensors and Switches. *Nanoscale Horiz.* **2018**, *3*, 35–44.
- (30) Meng, F.; Wang, M.; Lu, W.; Li, Q.; Chou, T.-W.; Zheng, L. An Electromechanical Behavior of Reduced Graphene Oxide Fiber. *Carbon* **2016**, *105*, 244–247.
- (31) Shi, G.; Zhao, Z.; Pai, J.-H.; Lee, I.; Zhang, L.; Stevenson, C.; Ishara, K.; Zhang, R.; Zhu, H.; Ma, J. Highly Sensitive, Wearable, Durable Strain Sensors and Stretchable Conductors Using Graphene/Silicon Rubber Composites. *Adv. Funct. Mater.* **2016**, *26*, 7614–7625.
- (32) Wang, Y.; Yang, R.; Shi, Z.; Zhang, L.; Shi, D.; Wang, E.; Zhang, G. Super-Elastic Graphene Ripples for Flexible Strain Sensors. *ACS Nano* **2011**, *5*, 3645–3650.
- (33) Zang, J.; Ryu, S.; Pugno, N.; Wang, Q.; Tu, Q.; Buehler, M. J.; Zhao, X. Multifunctionality and Control of the Crumpling and Unfolding of Large-Area Graphene. *Nat. Mater.* **2013**, *12*, 321–325.
- (34) Mu, J.; Hou, C.; Wang, G.; Wang, X.; Zhang, Q.; Li, Y.; Wang, H.; Zhu, M. An Elastic Transparent Conductor Based on Hierarchically Wrinkled Reduced Graphene Oxide for Artificial Muscles and Sensors. *Adv. Mater.* **2016**, *28*, 9491–9497.
- (35) Qin, Y.; Peng, Q.; Ding, Y.; Lin, Z.; Wang, C.; Li, Y.; Xu, F.; Li, J.; Yuan, Y.; He, X.; Li, Y. Lightweight, Superelastic, and Mechanically Flexible Graphene/Polyimide Nanocomposite Foam for Strain Sensor Application. *ACS Nano* **2015**, *9*, 8933–8941.
- (36) Wang, Z.; Shen, X.; Han, N. M.; Liu, X.; Wu, Y.; Ye, W.; Kim, J.-K. Ultralow Electrical Percolation in Graphene Aerogel/Epoxy Composites. *Chem. Mater.* **2016**, *28*, 6731–6741.
- (37) Wang, Z.; Liu, X.; Shen, X.; Han, N. M.; Wu, Y.; Zheng, Q.; Jia, J. J.; Wang, N.; Kim, J.-K. An Ultralight Graphene Honeycomb Sandwich for Stretchable Light-Emitting Displays. *Adv. Funct. Mater.* **2018**, *28*, No. 1707043.
- (38) Xu, R.; Lu, Y.; Jiang, C.; Chen, J.; Mao, P.; Gao, G.; Zhang, L.; Wu, S. Facile Fabrication of Three-Dimensional Graphene Foam/Poly (dimethylsiloxane) Composites and Their Potential Application as Strain Sensor. *ACS Appl. Mater. Interfaces* **2014**, *6*, 13455–13460.
- (39) Fu, X.-W.; Liao, Z.-M.; Zhou, J.-X.; Zhou, Y.-B.; Wu, H.-C.; Zhang, R.; Jing, G.; Xu, J.; Wu, X.; Guo, W.; Yu, D. Strain Dependent Resistance in Chemical Vapor Deposition Grown Graphene. *Appl. Phys. Lett.* **2011**, *99*, No. 213107.
- (40) Chen, M.; Duan, S.; Zhang, L.; Wang, Z.; Li, C. Three-Dimensional Porous Stretchable and Conductive Polymer Composites Based on Graphene Networks Grown by Chemical Vapour Deposition and PEDOT:PSS Coating. *Chem. Commun.* **2015**, *51*, 3169–3172.
- (41) Yang, T.; Zhang, H.; Wang, Y.; Li, X.; Wang, K.; Wei, J.; Wu, D.; Li, Z.; Zhu, H. Interconnected Graphene/Polymer Micro-Tube Piping Composites for Liquid Sensing. *Nano Res.* **2014**, *7*, 869–876.
- (42) Xiao, M.; Kong, T.; Wang, W.; Song, Q.; Zhang, D.; Ma, Q.; Cheng, G. Interconnected Graphene Networks with Uniform Geometry for Flexible Conductors. *Adv. Funct. Mater.* **2015**, *25*, 6165–6172.
- (43) Li, X.; Sun, P.; Fan, L.; Zhu, M.; Wang, K.; Zhong, M.; Wei, J.; Wu, D.; Cheng, Y.; Zhu, H. Multifunctional Graphene Woven Fabrics. *Sci. Rep.* **2012**, *2*, No. 395.
- (44) Li, X.; Zhang, R.; Yu, W.; Wang, K.; Wei, J.; Wu, D.; Cao, A.; Li, Z.; Cheng, Y.; Zheng, Q.; Ruff, R.; Zhu, H. Stretchable and Highly Sensitive Graphene-on-Polymer Strain Sensors. *Sci. Rep.* **2012**, *2*, No. 870.
- (45) Yang, T.; Wang, W.; Zhang, H.; Li, X.; Shi, J.; He, Y.; Zheng, Q.-S.; Li, Z.; Zhu, H. Tactile Sensing System Based on Arrays of Graphene Woven Microfabrics: Electromechanical Behavior and Electronic Skin Application. *ACS Nano* **2015**, *9*, 10867–10875.
- (46) Zhao, N.; Wang, Z.; Cai, C.; Shen, H.; Liang, F.; Wang, D.; Wang, C.; Zhu, T.; Guo, J.; Wang, Y.; Liu, X.; Duan, C.; Wang, H.; Mao, Y.; Jia, X.; Dong, H.; Zhang, X.; Xu, J. Bioinspired Materials: from Low to High Dimensional Structure. *Adv. Mater.* **2014**, *26*, 6994–7017.
- (47) Tseng, P.; Napier, B.; Zhao, S.; Mitropoulos, A. N.; Applegate, M. B.; Marelli, B.; Kaplan, D. L.; Omenetto, F. G. Directed Assembly of Bio-Inspired Hierarchical Materials with Controlled Nanofibrillar Architectures. *Nat. Nanotechnol.* **2017**, *12*, 474–480.
- (48) Wegst, U. G. K.; Bai, H.; Saiz, E.; Tomsia, A. P.; Ritchie, R. O. Bioinspired Structural Materials. *Nat. Mater.* **2015**, *14*, 23–36.
- (49) Ketten, S.; Buehler, M. J. Nanostructure and Molecular Mechanics of Spider Dragline Silk Protein Assemblies. *J. R. Soc., Interface* **2010**, *7*, 1709–1721.
- (50) Cranford, S. W. Increasing Silk Fibre Strength through Heterogeneity of Bundled Fibrils. *J. R. Soc., Interface* **2013**, *10*, No. 20130148.
- (51) Spöner, A.; Vater, W.; Monajembashi, S.; Unger, E.; Grosse, F.; Weissart, K. Composition and Hierarchical Organisation of a Spider Silk. *PLoS One* **2007**, *2*, No. e998.
- (52) Jonathan, A. K.; Olena, R.; Gary, G. L.; David, L. K. Spider silks and their applications. *Trends Biotechnol.* **2008**, *26*, 244–251.
- (53) Zheng, Q.; Ip, W. H.; Lin, X.; Yousefi, N.; Yeung, K. K.; Li, Z.; Kim, J.-K. Transparent Conductive Films Consisting of Ultralarge Graphene Sheets Produced by Langmuir–Blodgett Assembly. *ACS Nano* **2011**, *5*, 6039–6051.
- (54) Zheng, Q.; Li, Z.; Yang, J.; Kim, J.-K. Graphene Oxide-Based Transparent Conductive Films. *Prog. Mater. Sci.* **2014**, *64*, 200–247.
- (55) Farcau, C.; Sangeetha, N. M.; Moreira, H.; Viallet, B.; Grisolia, J.; Ciuculescu-Pradines, D.; Ressler, L. High-Sensitivity Strain Gauge Based on a Single Wire of Gold Nanoparticles Fabricated by Stop-and-Go Convective Self-Assembly. *ACS Nano* **2011**, *5*, 7137–7143.
- (56) Lee, J.; Shin, S.; Lee, S.; Song, J.; Kang, S.; Han, H.; Kim, S. G.; Kim, S.; Seo, J.; Kim, D. E.; Lee, T. Highly Sensitive Multifilament Fiber Strain Sensors with Ultrabroad Sensing Range for Textile Electronics. *ACS Nano* **2018**, *12*, 4259–4268.
- (57) Lin, Y.; Liu, S.; Chen, S.; Wei, Y.; Dong, X.; Liu, L. A Highly Stretchable and Sensitive Strain Sensor Based on Graphene–

Elastomer Composites with a Novel Double-Interconnected Network. *J. Mater. Chem. C* **2016**, *4*, 6345–6352.

(58) Samad, Y. A.; Li, Y.; Schiffer, A.; Alhassan, S. M.; Liao, K. Graphene Foam Developed with a Novel Two-Step Technique for Low and High Strains and Pressure-Sensing Applications. *Small* **2015**, *11*, 2380–2385.

(59) Deng, S. K.; Berry, V. Wrinkled, Rippled and Crumpled Graphene: an Overview of Formation Mechanism, Electronic Properties, and Applications. *Mater. Today* **2016**, *19*, 197–212.

(60) Wang, C. Y.; Xia, K. L.; Jian, M. Q.; Wang, H. M.; Zhang, M. C.; Zhang, Y. Y. Carbonized Silk Georgette as an Ultrasensitive Wearable Strain Sensor for Full-Range Human Activity Monitoring. *J. Mater. Chem. C* **2017**, *5*, 7604–7611.

(61) Yasuoka, T.; Shimamura, Y.; Todoroki, A. Electrical Resistance Change under Strain of CNF/Flexible Epoxy Composite. *Adv. Compos. Mater.* **2010**, *19*, 123–128.

(62) Shi, Z.; Lu, H.; Zhang, L.; Yang, R.; Wang, Y.; Liu, D.; Guo, H.; Shi, D.; Gao, H.; Wang, E.; Zhang, G. Studies of Graphene-based Nanoelectromechanical Switches. *Nano Res.* **2012**, *5*, 82–87.

(63) Zhang, J.; Jianwen, L.; Rongchuan, Z.; Edith, M.; Gert, H.; Shanglin, G. Single MWNT-Glass Fiber as Strain Sensor and Switch. *Adv. Mater.* **2011**, *23*, 3392–3397.

(64) Tolvanen, J.; Hannu, J.; Jantunen, H. Stretchable and Washable Strain Sensor Based on Cracking Structure for Human Motion Monitoring. *Sci. Rep.* **2018**, *8*, No. 13241.

(65) Tolvanen, J.; Hannu, J.; Palosaari, J.; Nelo, M.; Jantunen, H. Screen-Printed Mechanical Switch based on Stretchable PU-Foam Film. *Electron. Lett.* **2016**, *52*, 1395–1397.

(66) Liu, X.; Sun, X.; Wang, Z.; Shen, X.; Wu, Y.; Kim, J.-K. Planar Porous Graphene Woven Fabric/Epoxy Composites with Exceptional Electrical, Mechanical Properties, and Fracture Toughness. *ACS Appl. Mater. Interfaces* **2015**, *7*, 21455–21464.

(67) Shen, X.; Wang, Z.; Wu, Y.; Liu, X.; He, Y.-B.; Zheng, Q.; Yang, Q.-H.; Kang, F.; Kim, J.-K. A Three-Dimensional Multilayer Graphene Web for Polymer Nanocomposites with Exceptional Transport Properties and Fracture Resistance. *Mater. Horiz.* **2018**, *5*, 275–284.